MRI Study of Temperature Dependence of Multi-exponential Transverse Relaxation Times in Tomato

Rodolphe Leforestier, François Mariette, Maja Musse

▶ **To cite this version:**

Rodolphe Leforestier, François Mariette, Maja Musse. MRI Study of Temperature Dependence of Multi-exponential Transverse Relaxation Times in Tomato. Applied Magnetic Resonance, 2021, 10.1007/s00723-021-01374-7 . hal-03313774

HAL Id: hal-03313774
https://hal.inrae.fr/hal-03313774v1

Submitted on 18 Sep 2023

HAL is a multi-disciplinary open access archive for the deposit and dissemination of scientific research documents, whether they are published or not. The documents may come from teaching and research institutions in France or abroad, or from public or private research centers.

L'archive ouverte pluridisciplinaire **HAL**, est destinée au dépôt et à la diffusion de documents scientifiques de niveau recherche, publiés ou non, émanant des établissements d'enseignement et de recherche français ou étrangers, des laboratoires publics ou privés.

MRI study of temperature dependence of multi-exponential transverse relaxation times in tomato

Authors : Rodolphe Leforestier, François Mariette, Maja Musse

INRAE UR OPAALE, 17, rue de Cucillé, 35044 Rennes France.

Corresponding author: Maja MUSSE

Address : 17 avenue de Cucillé, CS 64427, 35044 Rennes, France

Telephone : +33 2 23 48 21 79

E-mail : maja.musse@inrae.fr

ORCID : 0000-0002-1681-5592

SUMMARY

The effects of the temperature on the multi-exponential transverse relaxation signal of fruit tissues was studied by MRI at 1.5T, with tomato as an example of fleshy fruits. The relative importance of chemical exchange mechanisms was investigated by comparing the results obtained from tomatoes with those obtained from aqueous solutions made up to simulate the vacuolar water pool. A more extended analysis of the effects of chemical exchanges on transverse relaxation time distributions was performed using the two-site Carver and Richards's expression, by fitting the experimental dispersion curves with the theoretical model.

At temperatures between 7 and 32 °C, the transverse relaxation signal in tomato pericarp was multi-exponential, indicating that cell membranes acted, at least partially, as barriers to diffusive exchanges of water molecules between cell compartments. Unexpectedly, the transition from two to three peaks in the T_2 distribution occurred between 7°C and 15°C for most of the tomatoes analyzed. Further, the relaxation time of the vacuolar water pool of the tomato pericarp remained mostly stable with temperature, which was contrary to expectations when only chemical exchange mechanisms were taken into account. It was deduced that additional mechanisms compensated for the expected increase in T_2 in the tomato pericarp. The hypotheses were discussed, in which the loss of the water magnetization at the membranes was assumed to be produced either by diffusive exchanges between compartments or by chemical exchanges between protons from water molecules and solid membranes.

Introduction

Time Domain Nuclear Magnetic Resonance (TD-NMR) and Magnetic Resonance Imaging (MRI) are unique in being able to provide information about subcellular water compartmentation in plant tissues [1]. Indeed, multi-exponential transverse relaxation decay, measured using TD-NMR or MRI optimal signal sampling [2], is able to reflect the behaviour of water protons in different environments. In plant tissues, it has generally been assumed that these proton pools correspond to water in main cell compartments i.e the vacuole, cytoplasm and wall and extracellular spaces. The bulk T_2 relaxation for each water pool largely depends on its composition (solute type and concentration) via the chemical exchanges of water protons with protons from solute molecules. The T_2 of water in cell compartments depends on the diffusion of water molecules between neighboring cell compartments separated by cell membranes that partially averages their NMR signals in the way that depends on the differences in their bulk relaxation times, water self-diffusion coefficients, compartment sizes and the water permeability of the membranes [3]. Further, the bulk T_2 could potentially be impacted by the exchanges of water protons with protons from non-soluble molecules such as proteins in bilayer phospholipid membranes that can act as relaxing solid surfaces. A number of studies have set out to explain these complex relaxation mechanisms and thereby characterize water distribution in plant tissues undergoing physiological changes [4-6] or subject to processing [7]. T_2 relaxation has been successfully used to investigate membrane damage in tissues undergoing thermal processing with a resultant loss of cell compartmentalization and tissue integrity [8-10]. However, the variations of relaxation time with temperature have been discussed only rarely with regard to the temperature range preceding phase change or cell denaturation [8,9]. Several relaxation mechanisms cause these variations with temperature. Changes in tissue temperature lead to variations in bulk T_2 for the water in cell compartments via both the dipole–dipole interactions of water molecules and chemical exchange mechanisms, as both molecular mobility and the rates of the chemical exchanges between water and solute protons are strongly dependent on temperature. Consequently, the relationship between bulk T_2 and the inverse of temperature, although linear for pure liquids, becomes complex in

plant cells [11]. In addition, temperature affects the water self-diffusion coefficient and membrane permeability, thus influencing the degree to which the relaxation signal of water in different cell compartments is partially averaged, and potentially impacts the surface relaxation.

In view of the phenomena described above, a number of difficulties can arise in interpreting changes in the transverse relaxation signal during the heating or cooling of plant tissues. Nevertheless, an accurate interpretation of the NMR relaxation signal would be of considerable interest if we are to benefit fully from MRI and TD-NMR approaches to the investigation of thermal transformations and heat stress in plant samples at the subcellular scale. In order to address this issue, the present study has set out to enhance understanding of the specific effects of temperature on multi-exponential transverse relaxation parameters. The experiments were performed on tomato, as a representative model for fleshy fruits, and were carried out within the temperature range that causes no damage to membranes (7-32°C) [12,13]. These temperatures also correspond to those experienced by plants in their natural environment. MRI relaxometry was used to measure relaxation times at different temperatures, by heating fruits directly in the MRI device. The MRI approach was chosen rather than TD-NMR, as this imaging mode is more suited to the investigation of whole fruit processing. The relative importance of chemical exchange and diffusional mechanisms was investigated by comparing the relaxation times measured in tomatoes with those of aqueous solutions created to simulate the vacuolar water pool, in accordance with the chemical composition of the pericarp tissue.

Materials and Methods

Plant material and solutions

Two separate MRI experiments (1 and 2) were conducted on tomato fruits in order to obtain consolidated data. For each experiment, five ripe tomatoes were purchased from the local market and used without any processing. The temperature set points were nearly the same in Experiments 1 and

2. In Experiment 2, additional measurements were performed in order to determine the chemical composition of cellular liquid. Following MRI acquisitions, the liquid phases were extracted by centrifugation from the outer pericarps sampled from each tomato. High pressure liquid chromatography (HPLC) analysis was then performed on the samples thus obtained to identify and quantify sugars and organic acids. The main solutes identified were glucose, fructose, citrate and malate at 13.7±1.6, 14.0±0.7, 3.7±0.6 and 0.3±0.2 $g.L^{-1}$ respectively and the pH value was 4.3±0.1 (mean value ± standard deviation obtained from liquid samples of four different tomatoes). These results are in agreement with the measurements reported in the literature [14-17]. It have to be noted that differences in pH exist between the different cellular compartments of the fruits [18]. Generally, the pH within the cytoplasm is neutral [19] while the pH of the vacuole is typically under 5.5 [20,21] due to the presence of H^+-ATPase and H^+-PPase membrane proteins which act as a proton pump in order to maintain this acidity for the proper functioning of the cell. In cherry tomatoes, vacuolar pH was shown to vary between 4.5 and 3.9 during fruit development [19]. pH of apoplastic liquid was found to be about 4.8 and 4.4 in pink and red mature tomato fruits [22]. Considering that the vacuolar water acts as a buffer solution [21] and that the liquid fractions from other cell compartments are significantly lower, it is reasonable to think that the pH measured in the extracted juice is close to that of the vacuole. A solution that simulated the vacuolar solution was prepared in accordance with the mean chemical composition and pH of the tomatoes by assuming that most of the sugars and acids found in the extracted liquid phase corresponded to those present in the vacuole [21]. A second solution was prepared with the same chemical composition but with a neutral pH to help the investigation of the effects of chemical exchanges on the transverse relaxation signal. These two solutions were obtained by dissolving sugars and acids in ultra-pure water (resistivity at 25°C: 18.2 MΩ.cm, Synergy UV Water Purification System, Merck, Darmstadt, Germany) and by adding sodium azide (2.0 mmol/L) as the antibacterial agent while stirring constantly. Sugars, organic and hydrochloric acids and sodium hydroxide were purchased from Sigma Chemicals and used as found without further purification. Five tubes (3.4 cm in diameter and 7.0 cm in height) were each filled with 50 ml of solution

(acid solution - 1 tube, neutral solution - 1 tube and pure water - 3 tubes). They were placed on a specially-designed base with 2mm-thick neoprene pads between the tubes and the base to prevent vibrations during MRI measurements.

Magnetic Resonance Imaging

Image acquisition

MRI measurements were performed on a 1.5T scanner (Magnetom Avanto, Siemens, Erlangen, Germany) equipped with a circular polarized head array RF coil. Tomatoes were placed in a temperature regulating device installed inside the RF coil. Five optical fibers connected to a data logger (UMI8, FISO Technologies Inc., Canada) were inserted into an additional tomato placed outside the Field of View (FOV), to monitor the temperature of the samples during the MRI experiment (Experiments 1 and 2). The experiment on the aqueous solutions was performed using the same MRI protocol, while the optical fibers were immersed in a beaker of water placed outside the FOV and close to the tubes. The MRI acquisition began when the temperature reached a steady value (about 1h30min after starting the temperature regulation). Prior to the experiment, the uncertainty of the temperature measurement was estimated to be less than 1°C.

Transverse relaxation parameters were measured in the tomatoes and the solutions using a multi-spin echo (MSE) sequence [23] with 256 echoes where the first echo (TE) was equal to the inter-echo spacing. Pixel bandwidth was 260Hz and one scan was performed. Repetition time (TR) was fixed at 20s in order to prevent T_1-weighting. The Apparent Diffusion Coefficient (ADC) was estimated using the pulse field gradient spin echo (PFGSE) sequence with TE=91ms, TR=5s, diffusion time Δ=60ms and diffusion gradient duration δ=20ms. Eight diffusion gradient strengths were applied, resulting in 8 b values ($b=\gamma^2G^2\delta^2(\Delta-\delta/3)$, with γ gyromagnetic ratio) ranging from 0 to 1197 $s.mm^{-2}$. Geometrical parameters were kept constant for both T_2 and ADC measurements. Transverse sections at the fruit's mid-height were imaged with a 5mm slice thickness, 152x152 pixels matrix and FOV = 152x152mm^2. T_2 and ADC measurements of tomatoes were carried out at four temperatures set at 7, 15, 24 and 32°C

and 8, 15, 23 and 31°C in Experiments 1 and 2 respectively. T_2 and ADC measurements of the solutions and the water were performed at temperatures of 9, 13, 17, 20, 27 and 35°C. The repeatability of the T_2 measurements, including the acquisition and image processing steps, was estimated in Experiment 2 by acquiring three scans at TE=6.5ms with separate scanner settings (automatic frequency and transmitter attenuation/gain adjustments and shimming) at 8°C. Standard deviation for the solutions and the water was less than 0.4% of the T_2 value measured in each tube. The repeatability of the diffusion measurements, including the acquisition and image processing steps, was tested at 20°C for the water and the solutions. The variation was less than 0.15% of the ADC value measured in each tube.

The impact of the vacuolar water pool composition on its bulk T_2 value, via the chemical exchange of protons from water and solutes, was investigated by measuring dispersion curves (T_2 measurements at different TE values) in the tomatoes and solutions. For the tomatoes, TE was set at 6.5, 8, 10, 12 and 20ms and at 6.5, 12 and 20ms in Experiments 1 and 2 respectively, with a TR of 20s and a single scan. Measurements were carried out at the lowest temperature analyzed (8 and 7°C for Experiments 1 and 2). For the solutions, dispersion curves were measured at 8, 12, 15, 20, 24, 28 and 32°C with TE set at 6.5, 7, 8, 9, 10, 12, 14, 16, 18 and 20ms, with a TR of 10s and a single scan.

The acquisition parameters for T_2 measurements are summarized in Table 1.

Image processing

Analysis focused on outer pericarp tissue as this is the less porous part of the tomato fruit [24], meaning that the effects of the diffusion of water in the random magnetic field gradients generated by the susceptibility-induced inhomogeneities that result from the presence of gas in intercellular spaces could be disregarded. Regions of interest (ROI) were selected manually using ImageJ software (National Institutes of Health, USA) on the outer pericarp of each fruit (Fig. 1). The mean signals of the ROIs were used to estimate T_2. The signal to noise ratio (SNR) was computed by dividing the ratio of

the mean signal of the ROI and the mean background signal by $\sqrt{\frac{\pi}{2}}$. Only data characterized by SNR greater than 7 were retained for the estimation of relaxation parameters, making it possible to assume a zero-mean Gaussian noise distribution in the magnitude images at all echo times. Because variations in temperature can lead to changes in the relaxation decay model for tomato pericarp, estimation of the relaxation parameters was carried out in Scilab software using a Maximum Entropy Method (MEM) [25], which provides a continuous distribution of relaxation times without assumptions concerning their number. The relaxation parameters and ADC of the solutions and water were estimated by fitting a mono-exponential T_2 and ADC maps on pixel-to pixel bases with Scilab software, using the Levenberg–Marquardt algorithm for chi-square minimization. The same procedure was used to compute ADC maps of the tomatoes. Parameter mean values were then estimated for the ROIs. For the tomatoes, ROIs were identical to those selected for the estimation of the multi-exponential T_2 (Fig. 1), while for the solutions, they corresponded to tube sections.

Results

Changes with temperature in transverse relaxation time distributions of tomato pericarp

The transverse relaxation time distributions for pericarp tissue in the four tomatoes analyzed in Experiment 1 are shown in Fig. 2. The distributions were described by two or three relaxation peaks depending on the temperature. At 7°C, two peaks could be distinguished for three of the four tomatoes analyzed in Experiment 1 (Figs. 2 A, C and D), with the shortest T_2 peaks centered at the value range of 50-90ms and representing a few percent of the total signal intensity while the T_2 value corresponding to the maximum amplitude for a second relatively large T_2 peak lay between 650 and 700ms. Note that asymmetry was observed in the second T_2 peak of the first and fourth tomatoes (Figs. 2A and D). For one tomato (Fig. 2B), an additional peak relaxing at about 350ms and representing about 18% of the signal could be distinguished. As the temperature increased, the first peak remained almost unchanged

while two other peaks (with long and medium T_2 values) were observed for all tomatoes. At 15°C, the second T_2 peak was centered at ~250ms and represented about 10% of the signal, while the longest T_2 peak was centered at ~650ms and represented about 88% of the signal. According to the literature [26] one hypothesis could be that the shortest, medium and longest T_2 peaks (T_{2S}, T_{2M} and T_{2L}, respectively) correspond to water located in the cell wall/extracellular water, cytoplasm and vacuolar compartments, respectively. However, the relative heterogeneity of the outer pericarp in terms of cell size [27,28], would rather support the hypothesis that the second and third peaks correspond to the vacuoles of two cell populations with distinct volume distributions, as has been observed in peach fruit [29] and oilseed rape leaves [30]. A relatively broad T_2 distribution observed in each experiment (Fig.2 and Supplementary Material 1), probably explained by cell size heterogeneity, is consistent with this hypothesis. The shortest T_2 peak (T_{2S}), could correspond to the non-vacuolar water (wall/extracellular water and cytoplasm) and/or to water in small vascular bundles. In most tomatoes studied, from 15 to 32°C, T_{2M} remained almost unchanged, while T_{2L} remained almost unchanged throughout the whole temperature range studied. A similar trend in T_2 distribution evolution with temperature was observed in Experiment 2 (Supplementary Material 1), except that T_{2L} increased between 8 and 15°C and that the decrease in T_{2M} occurred from 23 to 31°C. The T_2 value corresponding to the maximum amplitude and the peak areas taken from the relaxation time spectra for the tomatoes analyzed in Experiments 1 (Fig. 2) and 2 (Supplementary Material 1) are set out in Table 2. Similar trends of T_{2M} and T_{2L} with temperature between 15 and 31(32)°C, support the hypothesis that the second and third peaks correspond to vacuoles of different sizes, i. e. to compartments with similar composition and pH values (in opposite to what is expected if they represent pure cytoplasmic and vacuolar water, respectively). In Fig. 3, the sum of the signal intensities of the relaxation peaks measured in the tomato pericarp I(tot) is presented as a function of the inverse of temperature. I(tot) decreased linearly with the temperature as did the signals for the pure water and acid and neutral solutions, thus obeying Curie's law [31]. The fact that I(tot) decreased linearly with temperature, demonstrated that the same numbers of protons were contributing to the signal and that the TR applied ensured that T_1-weighting of the relaxation

signal was negligible in the temperature range studied. Therefore, given that in both experiments the relative intensity of the first peak remained almost unchanged, it can be deduced that the longest T_2 peak observed at the lowest temperatures (7/8°C) split into two peaks with temperature rise.

Evaluation of the effects of temperature on bulk transverse relaxation

If chemical exchanges between protons from water and solute molecules are the sole factor considered, the T_2 of the vacuolar liquid in tomato pericarp can be expected to increase linearly with temperature, in accordance with observations for sugar solutions at acidic pH under similar experimental conditions [11]. However, in the case of compartmented water pools such as those found in plant cells, it is important to consider not only the exchanges of water protons with the protons from solutes, but also diffusional exchanges of water molecules between neighboring compartments within the cell, as well as possible chemical exchanges of water protons with the protons from molecules within the membrane (phospholipids and proteins). In order to distinguish the contribution made by the effects of chemical exchanges on the bulk T_2 of the vacuolar liquid from those of other phenomena, the T_2 of the vacuolar liquid was compared to the T_2 of the simple systems (pure water and acid and neutral solutions with a chemical composition similar to that of the vacuolar liquid). The effects of chemical exchanges on transverse relaxation were assessed by measuring the dispersion curves (relaxation rate ($R_2=1/T_2$) as a function of 1/TE) at 8°C, as at lower temperature the impact of TE on T_2 was enhanced (Fig. 4). It can be observed that for the vacuolar liquid, R_{2L} as a function of TE remained nearly unchanged in both Experiments 1 and 2. R_2 for the acid solution, formulated to simulate the vacuolar liquid, also remained almost unchanged with the increase in TE. This was probably due to the high value of the exchange rate (k_b) between sugar and water protons compared to 1/TE observed for low pH values, leading to the fast exchange regime. By contrast, a marked decrease in R_2 was observed as TE increased from 6.5 to 20ms in the case of the solution with the same composition as that of the acid solution, but with a neutral pH. Indeed, for the neutral pH , k_b tends towards its minimum [32], leading to the slow exchange regime when ($k_b<<1/TE$) and the noticeable

dispersion effect in the echo time range analyzed. Last, as expected, the observed variations in water R_2 were insignificant (less than 2%) and were attributed to the diffusion of water molecules in the background and imaging gradients and to RF pulse imperfections. As these T_2-reducing contributions were considered to be similar in all systems studied, they were excluded from the analysis.

Although the dispersion curves measured in tomato pericarp and the acid solution showed similar trends, the relaxation rate of the acid solution was lower (~20%) than that of the vacuolar water pool. This difference was expected because 1) the vacuolar liquid did not contain only the soluble components found by the HPLC but probably also amino acids and paramagnetic ions; 2) its pH could be slightly higher than 4.4, as this value was determined from the extracted cell liquid by assuming that the vacuole represented the major part of the cell liquid (see Materials and Methods section) and 3) in addition to the proton exchanges between water and solute molecules, diffusional exchanges of water molecules between vacuole and cytoplasm and surface relaxation of water in contact with phospholipids and proteins from the tonoplast is thought to contribute to sink effect for water relaxation in the vacuole. Given the similar dispersion behavior of the slowest-relaxing component measured in the tomato pericarp and the acid solution (almost constant R_2), it was assumed that the acid solution provided a sufficiently accurate simulation of the bulk vacuolar water for further analysis to be carried out.

Additional insight into the chemical exchange effects on relaxation time distributions was gained by fitting the experimental dispersion curves measured for the solutions with the two-site expression of the Carver and Richards model [33] described in Appendix. Here, the following approximations were used: glucose and fructose were modelled as a single sugar and citrate and malate were disregarded due to their relatively low concentrations. It is true that, for a single sugar solution, each hydroxyl group does not necessarily have the same electronic environment and therefore the same chemical shift value. However, it has been demonstrated that $1/T_2$ of the 50:50 fructose and glucose solution is equal to the weighted $1/T_2$ average of the two pure sugar solutions at the same concentration and pH [11]. The fitting was carried out by using the Levenberg-Marquardt

algorithm in the Datafit function of the Scilab 5 software, as described in [11]. The fit was performed for the solution at neutral pH with the following outputs: solute exchangeable proton population (P_b), rate of proton exchange between water and solutes (k_b), difference in chemical shift between the protons from water and solutes ($\Delta\omega$, in ppm), and transverse relaxation time of solute protons (T_{2b}), with the water relaxation time (T_{2a}) fixed at the value recorded for 8°C (1.61s). The parameters estimated from the fitting were: P_b=0.0088, k_b=256s^{-1}, $\Delta\omega$=1.0ppm and T_{2b}=21ms. The values of P_b and k_b were in accordance with those obtained for fructose and glucose solutions at the same concentration, temperature and pH [11], while $\Delta\omega$ corresponded to the mean of glucose and fructose chemical shifts (0.8 and 1.2ppm respectively). As a result, for the relatively low chemical exchange rate of the neutral pH solution, the limit of the long echo times ($1/TE<<k_b/2$) was not reached and, consequently, T_2 varied significantly between TE=6.5ms and TE=20ms (from 625ms to 486ms). This indicates that, under these experimental conditions, the effects of chemical exchanges on the relaxation times are significantly impacted by TE. As shown in Supplementary Data 2, T_2 varied between TEs of 6.5ms and 20ms in the whole temperature range analyzed. In the case of the acid solution, it was not possible to fit the Carver and Richards's model on the experimental data, as variations in R_2 with 1/TE were too low. However, for P_b, $\Delta\omega$ and T_{2b} set to the values obtained from the fit corresponding to the neutral solution data, the best correspondence between the model and experimental data was found for k_b of about 6000s^{-1}. The increase in the exchange rate when the pH deviated from the neutral value, was expected in line with [32]. For the solution at acid pH, the almost constant R_2 between TEs of 6.5 and 20ms was explained by the considerably higher exchange rate when compared with the difference in the chemical shifts between water and solute protons ($k_b>>\delta\omega$, with $\delta\omega=2\pi B_0\Delta\omega$, where B_0 is the main magnetic field strength), thus indicating the fast exchange regime. Across the range of echo times explored, the long echo time limit was reached ($1/TE<< k_b$) leading to an R_2 plateau. Since k_b increases with temperature according to Eyring's law, the long echo time limit was reached for all temperatures above 8°C and, consequently, an R_2 plateau was observed across the whole temperature range (Supplementary data 2).

Fig. 5 shows the evolution of T_2 with the inverse of temperature for water and for the acid and neutral solutions, along with the longest T_2 peak associated with the vacuolar water compartments measured in the tomato pericarp (T_{2L}). The well-known linear relationship between $\ln(T_2)$ and the inverse of temperature (Arrhenius plot) was seen for pure water. This linear relationship was also observed for the acid solution, with a similar slope to that of the water, as expected in the case of the fast exchange regime [11,32]. By contrast, the T_2 of the neutral solution varied with temperature in a complex way, decreasing with the temperature rise from 9 to 15°C and then increasing up to 35°C. This was attributed to the transition between intermediate and fast regimes at temperatures over 15°C resulting from the increase in exchange rate during heating, which was much more pronounced than the increase in $\Delta\omega$. As a result, the dispersion curves (Supplementary Material 2) show a specific behavior.

For the vacuolar water pool in the tomato pericarp, T_{2L} remained stable in Experiment 1, while it increased only between 8 and 15°C in Experiment 2 (see Table 2). By comparing these results to those obtained from the acid solution, it could be deduced that additional mechanisms compensated for the expected increase in T_2 for the tomato pericarp.

Apparent diffusion coefficient

Fig. 6 shows the ADC maps for tomatoes at different temperatures. The placenta was easily distinguishable from other tomato tissues due to its lower ADC, while radial pericarp and locular tissues were discernible only on some tomatoes, resembling the observable features of the T_2-weighted images (Fig. 1). The diffusion coefficients measured in the tomatoes, solutions and water all showed a similar relationship with temperature, resulting in an ADC that doubled in value between 7°C and 32°C for tomatoes and 9°C and 35°C for solutions and water. Indeed, at the lowest temperatures analyzed, the ADC of the water, solutions and tomatoes was 1.44±0.01, 1.35x$10^{-9}$$m^2$.$s^{-1}$ and 1.17±0.01 x$10^{-9}$$m^2$.$s^{-1}$ respectively (Fig. 5), and reached 2.90±0.04x$10^{-9}$$m^2$.$s^{-1}$, 2.72x$10^{-9}$$m^2$.$s^{-1}$ and 2.23±0.07x$10^{-9}$$m^2$.$s^{-1}$ respectively at the highest temperatures analyzed. A possible explanation for the higher ADC values in

the solutions compared with those of the tomato pericarp is provided by the fact that the ADC was computed from a mono-exponential model assuming a single component because the experimental conditions did not allow the extraction of a multi-exponential diffusion signal. The ADC would therefore correspond to the average apparent diffusion coefficients of the two water relaxation components T_{2M} and T_{2L}. The component T_{2S} was not considered because of a significant T_2 weighting effect. The bias resulting from this approximation was estimated, taking into account the fact that at 20°C, the ADC of the T_{2M} and T_{2L} water compartments was about $1.9x10^{-9}m^2.s^{-1}$ and $1.4x10^{-9}m^2.s^{-1}$ respectively according to [34], and that these water pools represented, respectively, 80 and 20% of the total signal relaxing at 680 and 320ms (see experimental data from Table 1). By taking into account a non-negligible T_2-weighting effect for TE= 91ms, the bias was estimated to about 7%.

The same slope was observed for the linear relationship between the ADC and temperatures for tomatoes, water and solutions (Fig. 7). This indicates that, at the relatively short observation time employed (Δ=60ms), a free diffusion regime was observed in which the time was not sufficiently long for all the water molecules to reach the compartment boundaries. The vacuolated cells of tomato pericarp are relatively large, with a shortest dimension up to 200µm and a length perpendicular to the cuticle that falls within a range of up to 600–700µm [27]. For the higher ADC measured (that of pure water at 32°C), the upper limit for restricted diffusion was 31 µm, which was considerably lower than the smallest dimension of the tomato pericarp cells (200µm).

Discussion

The multi-exponential transverse relaxation signal at all temperatures analyzed indicated that water exchange between components was slow or intermediate with respect to T_2 and that the cell membranes therefore acted as barriers, at least partially. Unexpectedly, the transition from two to three peaks in the T_2 distribution occurred between 7(8)°C and 15°C for most of the tomatoes analyzed (Fig. 2). This differed from what had been observed in apple samples [8], where the number of T_2 peaks for temperatures between 5 and 22°C remained unchanged. On the other hand, and in contrast to the

T_2 of the acid solution simulating vacuolar bulk relaxation, T_{2L} (Table 2, Fig. 5) remained stable with temperature (Experiment 1) or changed only between 8 and 15°C (Experiment 2). This means that the relationship between T_{2L} and temperature cannot be explained by the chemical exchanges between the water and the solutes dissolved in the vacuolar fluid. One mechanism that might give rise to these unexpected results is the loss of the water magnetization at the membrane. The degree of T_2 reduction depends on the surface to volume ratio of the compartment and the surface relaxivity of the membranes (ρ_2). The hypothesis that the loss of the magnetization of vacuolar water molecules at the membrane is due to the passage of the membrane and entry into the cytoplasm with considerably shorter T_2, and that ρ_2 of the vacuolar compartment is linearly related to the water permeability of the tonoplast, has been put forward in [35]. Temperature increase modifies cell membrane lipid interactions [36] impacting cell membrane permeability and fluidity [37] and would therefore favor diffusive exchange of molecules between neighboring compartments. This means that at increasing temperature, the diffusion exchange between compartments would be enhanced, due to cumulative effects of changes in membrane permeability and the increase in diffusion coefficient. Under the assumption that the second and third peaks correspond to the vacuoles of two cell populations with distinct volume distributions, the changes in diffusive exchange between the vacuole and cytoplasm compartments with relatively concentrated fluid potentially affects relaxation in all compartments, and would be emphasized for second peak (T_{2M}) attributed to water is smaller vacuoles. Moreover, T_2 of cytoplasm liquid characterized by neutral pH [19] could potentially be reduced with increasing temperature, resulting in an increased sink effect for water relaxation in the vacuole. These phenomena related to the loss of the magnetization of vacuolar water molecules at the membrane may partially explain the transition from two to three peaks in the T_2 distribution occurred between 7(8)°C and 15°C. It might also be possible that the temperature impacts characteristics of membrane proteins, which would affect the chemical exchange between protons from proteins embedded in the phospholipid bilayer of the membranes and vacuole liquid, thus modifying the membrane sink NMR relaxation. In this case, the same reasoning applies to relaxation peaks (T_{2M} and T_{2L}) attributed to

vacuoles of two cell populations with distinct volume distributions. Further in-depth investigations would be necessary to elucidate the mechanisms at the origin of the loss of the water magnetization at the membrane, particularly by taking into account the relatively large size of tomato pericarp cells. Another important consideration is that the vacuolar pH, considered to be constant over the entire temperature range explored in this study, could potentially change with temperature [38,39] due to modifications in the activity of the proteins (H^+-ATPase and H^+-PPase) regulating the acidity within the vacuole. In this case, slight variations of pH [32,40] could also impact significantly the variations in vacuolar liquid T_2.

A comparison of the results of the present experiment with the small number of studies from the literature addressing the dependence of relaxation time on temperature reveals the relationship between the multi exponential relaxation times and temperature to be complex [8,9]. Indeed, divergent results have been reported in the literature. Hills et al. [8] showed that an increase in the temperature of the apple parenchyma from 5°C to 22°C resulted in an increase in the T_2 of the vacuole liquid from 521 to 652ms. However, given the acid pH of apples [41] and the experimental conditions (TD-NMR, 100MHz, TE=0.4ms) favoring the fast exchange regime, more marked changes in T_2 with temperature might be expected [40]. In potato tubers [9], a decrease in T_2 measured by TD-NMR (23.2MHz, TE=0.3ms) was observed for both short and long components between 25 and 45°C, the long component decreasing from 450 to 375ms. This decrease in T_2 was interpreted as being caused by the increase in the exchange rate between the protons from water molecules and from hydroxyls in the starch. It has been demonstrated that the relationship between T_2 and temperature is complex when there is a shift in chemical exchanges regime, defined by the ratio $k_b/\delta\omega$, from fast to slow regime [11]. However, at low field and for the relatively high temperature range analyzed in [9], it seems unlikely that the chemical exchange regime deviates from the fast regime as it might at high field.

In this study, the effects of temperature on relaxation times were evaluated using MR imaging, which enables further investigations into thermal transformations in fleshy fruits. Indeed, the imaging approach has the advantage of being non-invasive, and the follow-up to the experiment can be carried

out using the same processing samples. In applying the conclusions to different experimental conditions, all variables relative to the tissues under investigations and the MRI experiment should be taken into account.

Conclusion

The present study demonstrated the complexity of the relationship between multi-exponential relaxation times and temperature in compartmentalized structures such as the pericarp tissue of fleshy fruits. Counter-intuitively, the increase in temperature made it possible to better distinguish the different T_2 components associated with water pools, reflecting cell compartmentation and probably tissue heterogeneity. The contributions of chemical exchange mechanisms to bulk transverse relaxation, analyzed by comparing the results obtained from tomatoes and from aqueous solutions simulating vacuolar liquid, showed that an additional mechanism contributes to the relationship between vacuolar T_2 and temperature. The hypotheses that the loss of the water magnetization at the membrane explain the unexpected dependence of T_2 on temperature is discussed. The monitoring and understanding of the role of the temperature variations in the NMR signal has relevance for processing and outdoor measurements, as variations in plant temperature affecting the relaxation signal have the potential to induce interpretation errors.

Acknowledgements

We are most grateful to the PRISM core facility (Rennes-Angers, France) for its technical support and to the GIS Biogenouest.

Declarations

Funding

This work was in part funded by the Région Bretagne.

Conflicts of interest

The authors have no conflicts of interest to declare.

Availability of data and material

All summary data are included in the article. Please contact the corresponding author for access to original images and data files.

Code availability

Not applicable.

Captions

Fig. 1: T_2-weighted (TE=793ms) image of tomato acquired with an MSE sequence (TR=20s, pixel size=1.2²mm² and slice thickness=5mm). The region of interest (ROI, outlined in green) was selected manually for each fruit from the outer pericarp.

Fig. 2: Transverse relaxation time distribution in tomato pericarp at different temperatures (— 7°C, — 15°C, — 24°C, — 32°C), calculated from MSE images (TR=20s, TE=6.5ms, pixel size=1.2²mm² and slice thickness=5mm). The data shown correspond to the tomatoes numbered 1 to 4 (left to right and top to bottom) analyzed in Experiment 1.

Fig. 3: Total signal intensity versus inverse of temperature measured using the MSE sequence (TR=20s, TE=6.5ms, 256 echoes, pixel size=1.2²mm² and slice thickness=5mm) in tomato pericarp (✖Experiment 1, ✖Experiment 2), acid (●pH 4.4) and neutral (●pH 7.0) solutions, and water (●). For each temperature, the signal was normalized using its value at 7(8)°C as a reference.

Fig. 4: Transverse relaxation dispersion curves for the longest T_2 component (T_{2L}) measured in the tomato pericarp (✖Experiment 1, ✖Experiment 2), the acid (●pH 4.4) and neutral (●pH 7.0) solutions, and water (●). T_2 relaxation times were measured using the MSE sequence (TR=20s, pixel size=1.2²mm² and slice thickness=5mm). Solid lines show least square fits of the Carver-Richard model to the experimental data.

Fig. 5: Ln(T_2) versus temperature inverse for the longest T_2 component (T_{2L}) measured in the tomato pericarp (✖Experiment 1, ✖Experiment 2), in the acid (●pH4.4) and neutral (●pH7.0) solutions, and water (●). T_2 relaxation times were measured using the MSE sequence (TR=20s, pixel size=1.2²mm² and slice thickness=5mm).

Fig. 6: Apparent diffusion coefficient (ADC) maps calculated at 8, 15, 23 and 31°C (Experiment 2), from left to right and top to bottom respectively. ADC was estimated using the PFGSE sequence (pixel size=1.2²mm² and slice thickness=5mm) with TE=91ms, TR=5s, diffusion time Δ=60ms, diffusion gradient duration δ=20ms and 8 diffusion gradient strengths, resulting in b values ($b=\gamma^2G^2\delta^2(\Delta-\delta/3)$ ranging from 0 to 1197 $s.mm^{-2}$.

Fig. 7: Apparent diffusion coefficient (ADC) versus temperature inverse for the tomato pericarp (●Experiment 1, ●Experiment 2), for the acid (●pH 4.4) and neutral (●pH 7.0) solutions and water (●). ADC was estimated using the PFGSE sequence (pixel size=1.2²mm² and slice thickness=5mm) with TE=91ms, TR=5s, diffusion time Δ=60ms, diffusion gradient duration δ=20ms and 8 diffusion gradient strengths, resulting in b values ($b=\gamma^2G^2\delta^2(\Delta-\delta/3)$ ranging from 0 to 1197 $s.mm^{-2}$.

Table 1: The acquisition parameters for T_2 measurements on tomatoes and model solutions. ADC measurements were carried out at the same temperatures.

Table 2: Mean T_2 values and corresponding relative intensities for four tomatoes measured using the MSE sequence (TR=20s, TE=6.5ms, 256 echoes, pixel size=1.2²mm² and slice thickness=5mm) and calculated by the MEM algorithm. Values are the means ± SD of the four tomatoes in each experiment at 7(8), 15, 24(23), and 32(31)°C respectively.

Supplementary Information 1: Transverse relaxation time distribution in the tomato pericarp at different temperatures (— 7°C, — 15°C, — 24°C, — 32°C), calculated from MSE images (TR=20s, TE=6.5ms, pixel size=1.2²mm² and slice thickness=5mm). The data shown correspond to the tomatoes numbered 1 - 4 (left to right and top to bottom) analyzed in Experiment 2.

Supplementary Information 2: Transverse relaxation dispersion curves for the acid (orange symbols pH 4.4) and neutral (red symbols pH 7.0) solutions and for water (blue symbols) at ●8, ◆15, ✖24 and ■32°C. T_2s were measured using the MSE sequence (TR=20s, TE=6.5ms, 256 echoes, pixel size=1.2²mm² and slice thickness=5mm). Solid lines show least square fits of the Carver-Richards model to the experimental data.

REFERENCES

[1] H. Van As, J. van Duynhoven, Journal of Magnetic Resonance 229 (2013) 25.

[2] H. Adriaensen, M. Musse, S. Quellec, A. Vignaud, M. Cambert, F. Mariette, Magn Reson Imaging 31 (2013) 1677.

[3] L. Van Der Weerd, M.M.A.E. Claessens, C. Efdé, H. Van As, Plant, Cell & Environment 25 (2002) 1539.

[4] M. Musse, K. Bidault, S. Quellec, B. Brunel, G. Collewet, M. Cambert, N. Bertin, The Plant Journal (2020).

[5] A. Raffo, R. Gianferri, R. Barbieri, E. Brosio, Food Chemistry 89 (2005) 149.

[6] C. Sorin, F. Mariette, M. Musse, L. Leport, F. Cruz, J.-C. Yvin, Applied Sciences 8 (2018) 943.

[7] B.P. Hills, K.P. Nott, Appl Magn Reson 17 (1999) 521.

[8] B.P. Hills, B. Remigereau, International journal of food science & technology 32 (1997) 51.

[9] M. Mortensen, A.K. Thybo, H.C. Bertram, H.J. Andersen, S.B. Engelsen, Journal of agricultural and food chemistry 53 (2005) 5976.

[10] M.E. Gonzalez, D.M. Barrett, M.J. McCarthy, F.J. Vergeldt, E. Gerkema, A.M. Matser, H. Van As, Journal of food science 75 (2010) E417.

[11] R. Leforestier, F. Mariette, M. Musse, Journal of magnetic resonance (2020) 106872.

[12] P. Ilík, M. Špundová, M. Šicner, H. Melkovičová, Z. Kučerová, P. Krchňák, T. Fürst, K. Večeřová, K. Panzarová, Z. Benediktyová, New Phytologist 218 (2018) 1278.

[13] P. Ahmad, M.N.V. Prasad, Environmental adaptations and stress tolerance of plants in the era of climate change, Springer Science & Business Media, 2011.

[14] J. Osvald, N. Petrovic, J. Demsar, Acta Alimentaria 30 (2001) 53.

[15] A. Adekunte, B. Tiwari, P. Cullen, A. Scannell, C. O'donnell, Food Chemistry 122 (2010) 500.

[16] C. Agius, S. von Tucher, B. Poppenberger, W. Rozhon, MethodsX 5 (2018) 537.

[17] M.A. Stevens, A.A. Kader, M. Albright-Holton, Journal of the American Society for Horticultural Science 102 (1977) 689.

[18] W.G. Hopkins, Introduction to plant physiology, John Wiley and Sons, 1999.

[19] D. Rolin, P. Baldet, D. Just, C. Chevalier, M. Biran, P. Raymond, Functional Plant Biology 27 (2000) 61.

[20] L. Taiz, Journal of Experimental Biology 172 (1992) 113.

[21] K. Shiratake, E. Martinoia, Plant Biotechnology 24 (2007) 127.

[22] D.P. Almeida, D.J. Huber, Physiologia plantarum 105 (1999) 506.

[23] H. Adriaensen, M. Musse, S. Quellec, A. Vignaud, M. Cambert, F. Mariette, Magnetic resonance imaging 31 (2013) 1677.

[24] M. Musse, F. De Guio, S. Quellec, M. Cambert, S. Challois, A. Davenel, Magnetic resonance imaging 28 (2010) 1525.

[25] F. Mariette, J. Guillement, C. Tellier, P. Marchal, Data handling in science and technology, Elsevier, 1996, p. 218.

[26] J. Snaar, H. Van As, Biophysical Journal 63 (1992) 1654.

[27] D. Legland, M.F. Devaux, B. Bouchet, F. Guillon, M. Lahaye, Journal of Microscopy 247 (2012) 78.

[28] M. Lemaire-Chamley, F. Mounet, C. Deborde, M. Maucourt, D. Jacob, A. Moing, Metabolites 9 (2019) 93.

[29] M. Musse, K. Bidault, S. Quellec, B. Brunel, G. Collewet, M. Cambert, N. Bertin, The Plant Journal 105 (2021) 62.

[30] C. Sorin, M. Musse, F. Mariette, A. Bouchereau, L. Leport, Planta 241 (2015) 333.

[31] J.M. Coey, Magnetism and magnetic materials, Cambridge university press, 2010.

[32] B.P. Hills, Journal of the Chemical Society, Faraday Transactions 86 (1990) 481.

[33] J. Carver, R. Richards, Journal of Magnetic Resonance (1969) 6 (1972) 89.

[34] F.P. Duval, M. Cambert, F. Mariette, Applied Magnetic Resonance 28 (2005) 29.

[35] L. van der Weerd, M.M. Claessens, T. Ruttink, F.J. Vergeldt, T.J. Schaafsma, H. Van As, Journal of Experimental Botany 52 (2001) 2333.

[36] A. Blicher, K. Wodzinska, M. Fidorra, M. Winterhalter, T. Heimburg, Biophysical journal 96 (2009) 4581.

[37] Y. Niu, Y. Xiang, Frontiers in plant science 9 (2018) 915.

[38] G. Lester, E. Stein, Journal of the American Society for Horticultural Science 118 (1993) 223.

[39] M. Janicka-Russak, K. Kabała, A. Wdowikowska, G. Kłobus, Journal of plant research 125 (2012) 291.

[40] R. Leforestier, F. Mariette, M. Musse, Journal of magnetic resonance 322 (2021) 106872.

[41] J. Hou, Y. Zhang, Y. Sun, N. Xu, Y. Leng, Journal of food science 83 (2018) 661.

[42] B. Hills, K. Wright, P.S. Belton, Molecular Physics 67 (1989) 1309.

Fig. 1

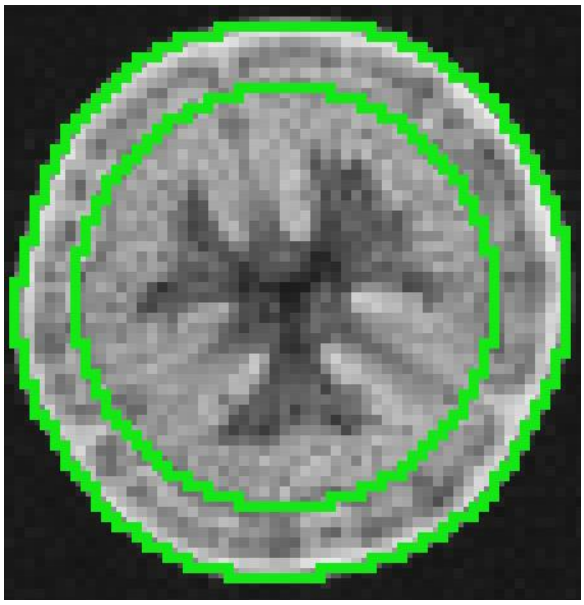

Fig. 2

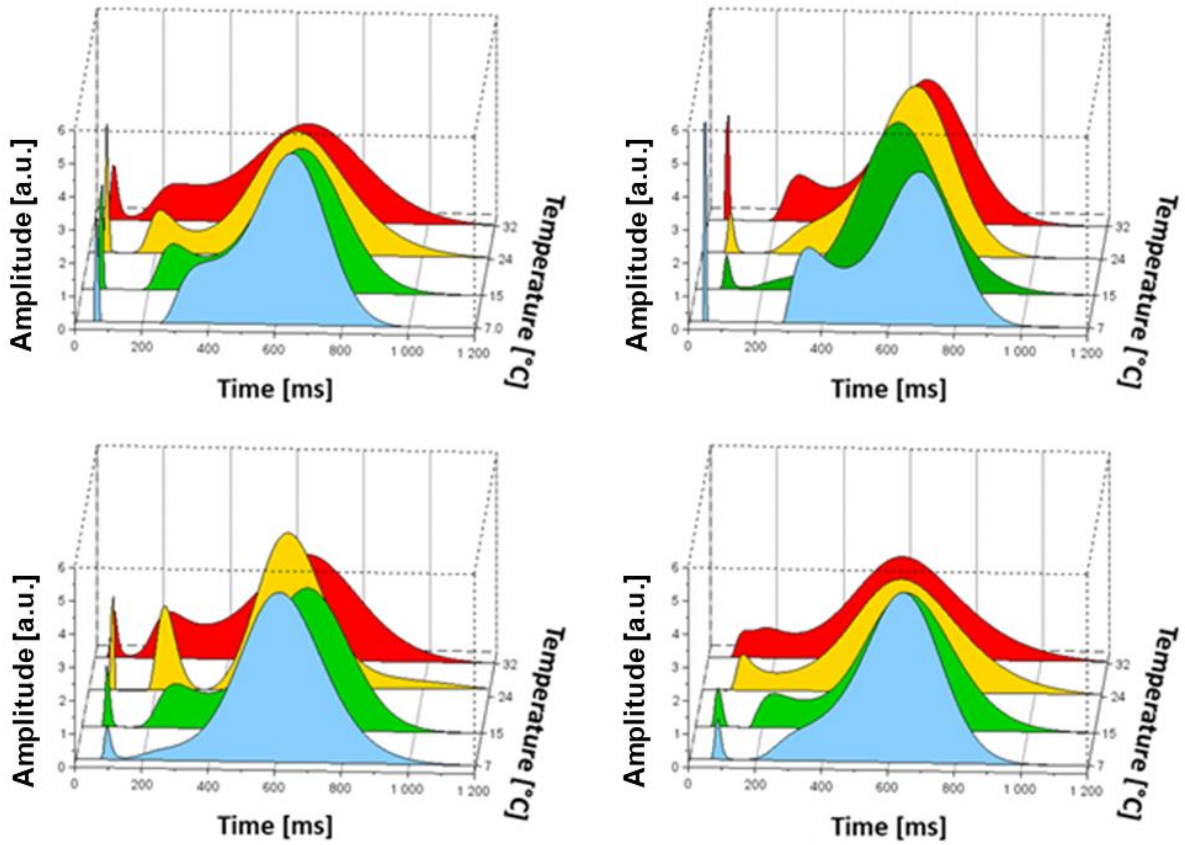
Amplitude [a.u.]
Time [ms]
Temperature [°C]
0
200
400
600
800
1 000
1 200
1
2
3
4
5
6
7.0
7
15
24
32

Fig. 3

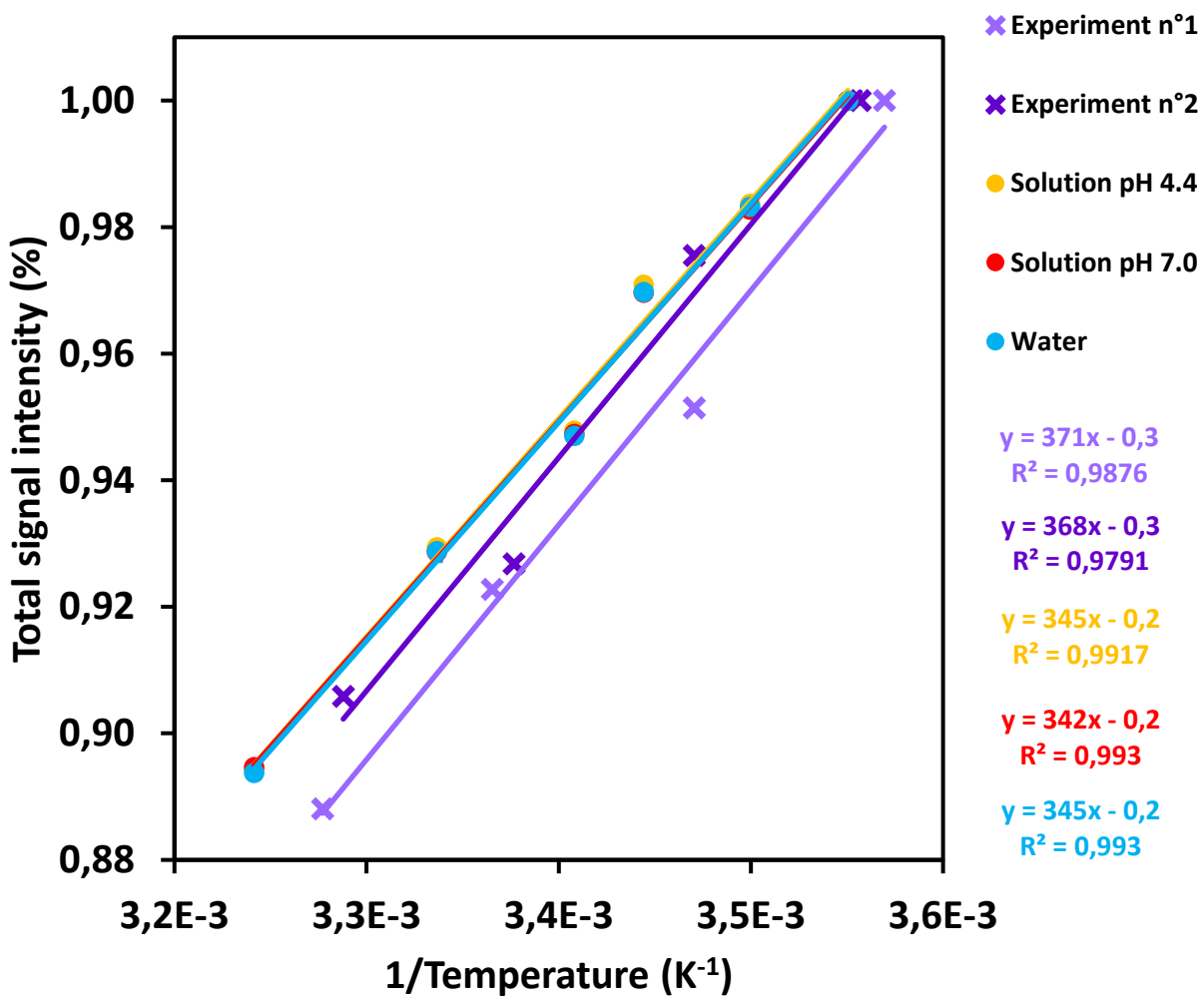
Experiment n°1
Experiment n°2
Solution pH 4.4
Solution pH 7.0
Water
y = 371x - 0,3
R² = 0,9876
y = 368x - 0,3
R² = 0,9791
y = 345x - 0,2
R² = 0,9917
y = 342x - 0,2
R² = 0,993
y = 345x - 0,2
R² = 0,993
Total signal intensity (%)
1,00
0,98
0,96
0,94
0,92
0,90
0,88
3,2E-3
3,3E-3
3,4E-3
3,5E-3
3,6E-3
1/Temperature (K-1)

Fig. 4

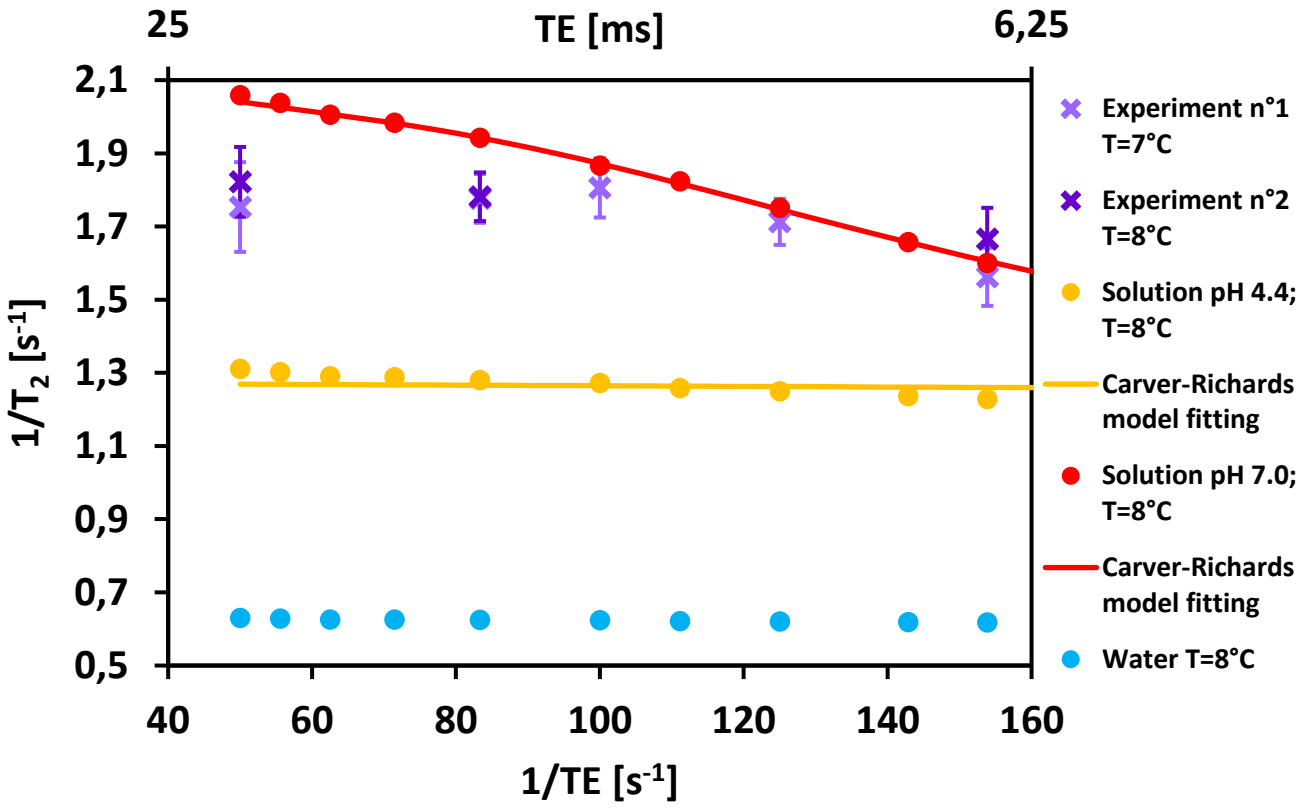
25
TE [ms]
6,25
2,1
1,9
1,7
1,5
1,3
1,1
0,9
0,7
0,5
1/T2 [s-1]
40
60
80
100
120
140
160
1/TE [s-1]
Experiment n°1 T=7°C
Experiment n°2 T=8°C
Solution pH 4.4; T=8°C
Carver-Richards model fitting
Solution pH 7.0; T=8°C
Carver-Richards model fitting
Water T=8°C

Fig. 5

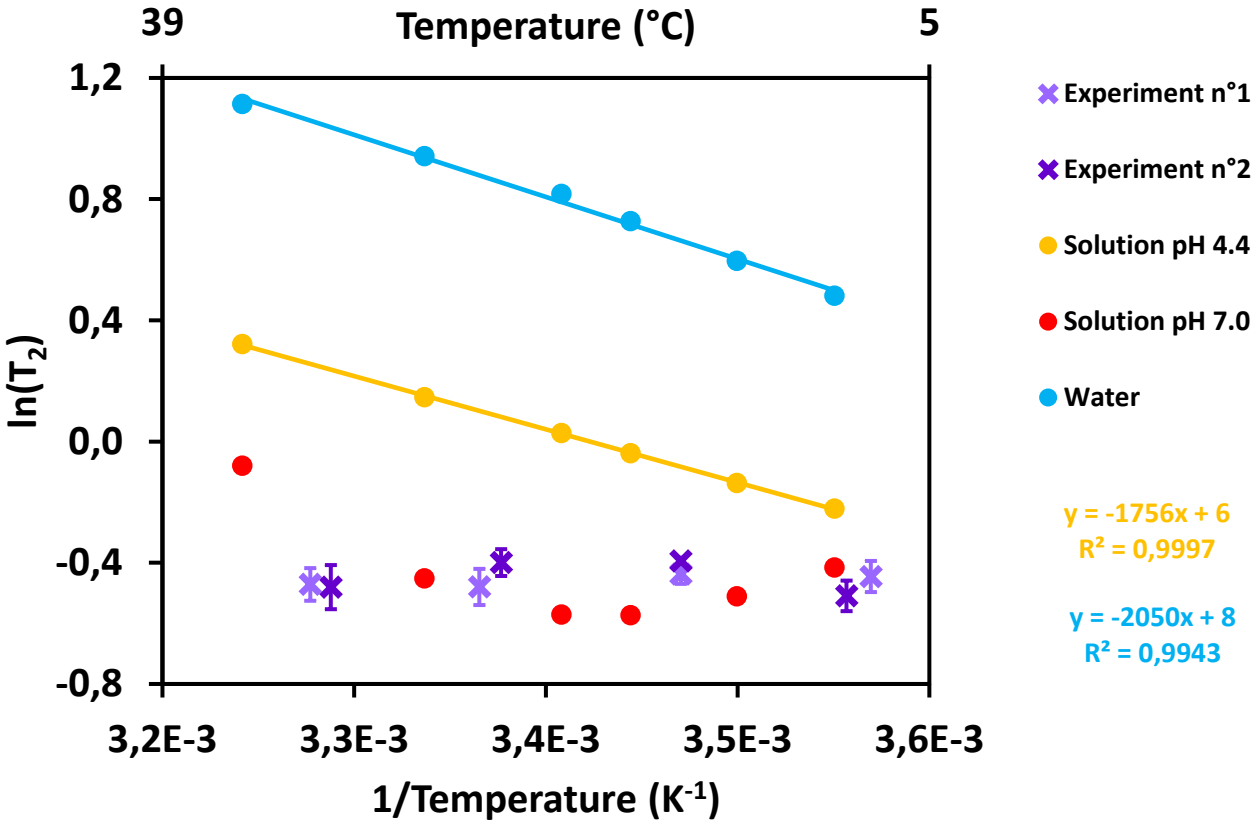
39
Temperature (°C)
5
1,2
0,8
0,4
0,0
-0,4
-0,8
ln(T2)
3,2E-3
3,3E-3
3,4E-3
3,5E-3
3,6E-3
1/Temperature (K-1)
Experiment n°1
Experiment n°2
Solution pH 4.4
Solution pH 7.0
Water
y = -1756x + 6
R² = 0,9997
y = -2050x + 8
R² = 0,9943

Fig. 6

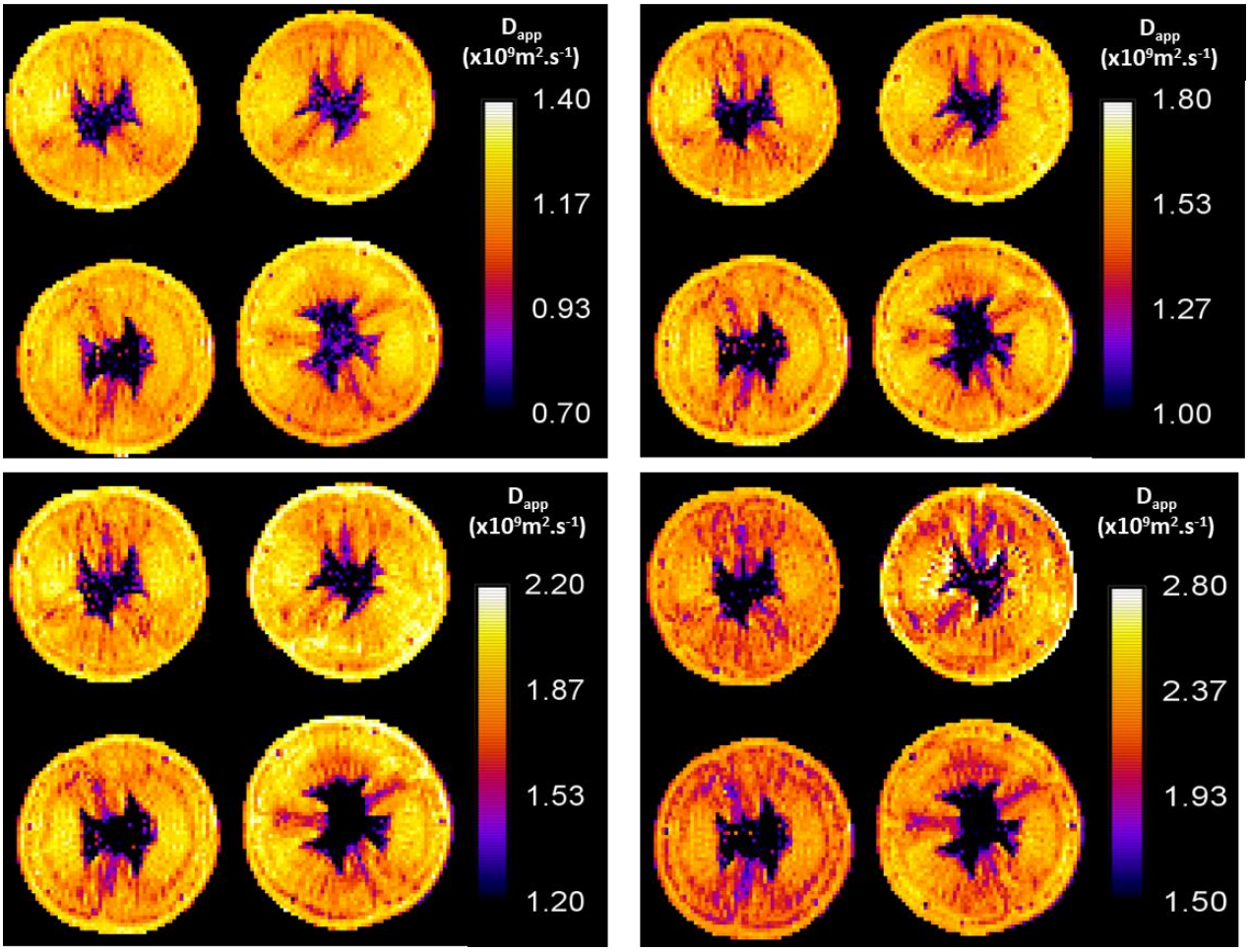
D_{app} ($x10^{9}m^{2}.s^{-1}$)
1.40
1.17
0.93
0.70
D_{app} ($x10^{9}m^{2}.s^{-1}$)
1.80
1.53
1.27
1.00
D_{app} ($x10^{9}m^{2}.s^{-1}$)
2.20
1.87
1.53
1.20
D_{app} ($x10^{9}m^{2}.s^{-1}$)
2.80
2.37
1.93
1.50

Fig. 7

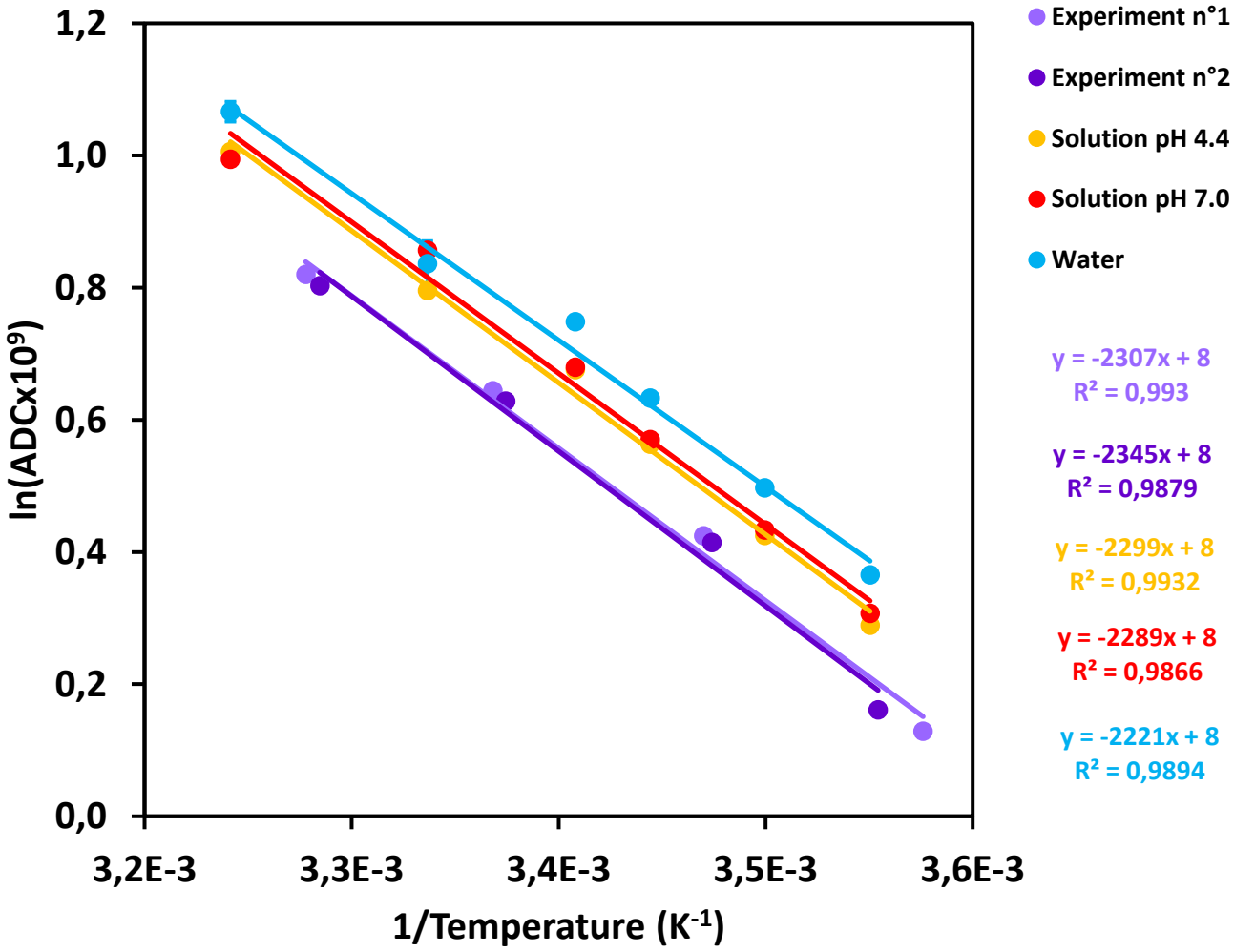
1,2
1,0
0,8
0,6
0,4
0,2
0,0
ln(ADCx10⁹)
3,2E-3
3,3E-3
3,4E-3
3,5E-3
3,6E-3
1/Temperature (K⁻¹)
Experiment n°1
Experiment n°2
Solution pH 4.4
Solution pH 7.0
Water
y = -2307x + 8
R² = 0,993
y = -2345x + 8
R² = 0,9879
y = -2299x + 8
R² = 0,9932
y = -2289x + 8
R² = 0,9866
y = -2221x + 8
R² = 0,9894

Table 1

TE (ms)	Temperature (°C)				Number of scans	TR (s)
EXPERIMENT 1 (tomatoes)						
6.5	7	15	24	32	3 at 7°C; 1 at 15, 24 and 32°C	20
8	7				1	
10						
12						
20						
EXPERIMENT 2 (tomatoes)						
6.5	8	15	23	31	3 at 8°C	20
12	8				1	
20						
EXPERIMENT ON SOLUTIONS						
6.5	8	15	24	32	3	10
7	8	15	24	32	1	
8						
10						
12						
14						
16						
18						
20						

Table 2

Temperature (°C)	I_{0S} (%)	T_{2S}(ms)	I_{0M}(%)	T_{2M} (ms)	I_{0L} (%)	T_{2L}(ms)
EXPERIMENT 1						
7	2 ± 1	62 ± 22			98 ± 1	626 ± 18
15	3 ± 1	48 ± 15	9 ± 3	255 ± 18	88 ± 2	646 ± 21
24	3 ± 1	51 ± 14	12 ± 3	224 ± 20	85 ± 5	629 ± 41
32	4 ± 2	47 ± 7	14 ± 4	233 ± 13	82 ± 5	640 ± 18
EXPERIMENT 2						
8	3 ± 1	73 ± 7			97 ± 1	593 ± 31
15	3 ± 1	71 ± 4	12 ± 4	315 ± 22	85 ± 5	675 ± 8
23	4 ± 1	60 ± 7	19 ± 5	321 ± 40	77 ± 6	680 ± 31
31	4 ± 1	47 ± 12	14 ± 4	226 ± 35	82 ± 5	629 ± 51

APPENDIX

The effects of chemical exchange between two spin species (a, b) in homogeneous sugar systems can be estimated using the theoretical dispersion curves (variation of relaxation rate with interpulse spacing of the Carr-Purcell-Meiboom-Gill (CPMG) pulse sequence) provided by the Carver and Richard's equations and corrected by Hills [33,42]:

- $\frac{1}{\mathrm{T}_2} = -\frac{1}{\mathrm{TE}}\ln\lambda_1$
- $\ln\lambda_1 = -\mathrm{TE}\frac{\alpha_+}{2} + \ln\left[\sqrt{\mathrm{D}_+.\cosh^2\xi - \mathrm{D}_-.\cos^2\eta} + \sqrt{\mathrm{D}_+.\sinh^2\xi + \mathrm{D}_-.\sin^2\eta}\right]$

with:

- TE : echo time (time between two 180° RF pulses)
- $\alpha_+ = \frac{1}{T_{2a}} + \frac{1}{T_{2b}} + k_a + k_b$
- $\alpha_- = \frac{1}{T_{2a}} - \frac{1}{T_{2b}} + k_a - k_b$
- T_{2a} and T_{2b} : transverse relaxation times of the water protons and the exchangeable protons of the solute respectively.
- τ_a and τ_b : lifetimes of states a and b respectively.
- $k_a = \frac{1}{\tau_a}$ and $k_b = \frac{1}{\tau_b}$: exchange rates at sites a and b respectively. ($k_a = \frac{P_b}{P_a}k_b$)
- P_a and P_b : fractions of the total proton population at sites a and b respectively.
  ($P_a = 1 - P_b$) and $P_b = \frac{number\ of\ exchangeable\ protons\ of\ the\ solute}{number\ of\ protons\ exchangeable\ in\ the\ solution\ (solvent + solute)}$
- $2D_+ = 1 + \frac{\psi + 2\Delta\omega^2}{\sqrt{(\psi^2 + \zeta^2)}}$
- $2D_- = -1 + \frac{\psi + 2\Delta\omega^2}{\sqrt{(\psi^2 + \zeta^2)}}$
- $\Delta\omega = \omega_b - \omega_a$: Chemical shift difference given in units of radial frequency rad s^{-1}.
- $\psi = \alpha_-^2 - \Delta\omega^2 + 4k_ak_b$
- $\zeta = 2\Delta\omega.\alpha_-$
- $\xi = \left(\frac{TE}{2\sqrt{2}}\right)\left[\psi + (\psi^2 + \zeta^2)^{\frac{1}{2}}\right]^{\frac{1}{2}}$
- $\eta = \left(\frac{TE}{2\sqrt{2}}\right)\left[-\psi + (\psi^2 + \zeta^2)^{\frac{1}{2}}\right]^{\frac{1}{2}}$

The chemical shift $\Delta\omega$ is given in units of radial frequency (rad s^{-1}): $\Delta\omega = 2\pi \times B_0 \times \delta\omega$, where $\delta\omega$ is the chemical shift difference between the two sites a and b in ppm.

Supplementary data 1

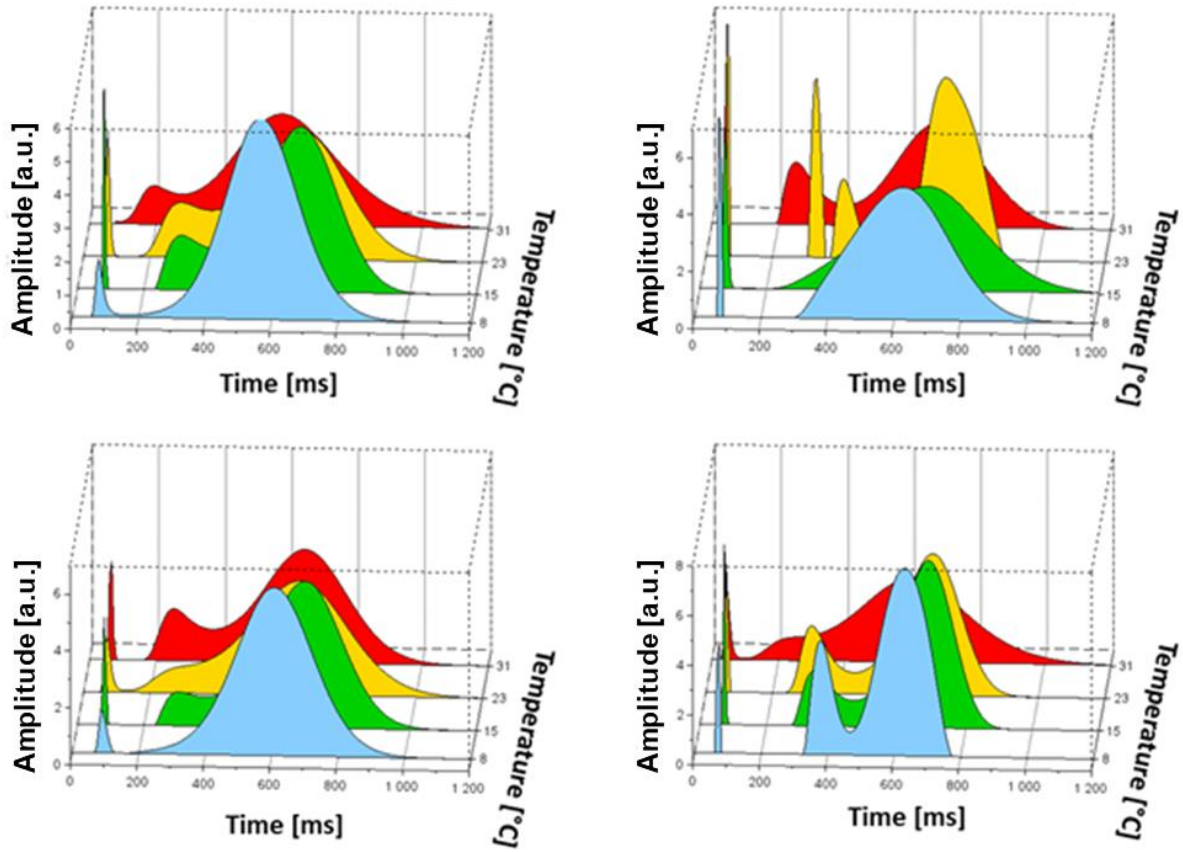

Supplementary data 2